Int J Adv Manuf Technol (2015) 80:1197–1211
DOI 10.1007/s00170-015-7024-3

ORIGINAL ARTICLE

Monte Carlo simulation and experimental measurements of grain growth in the heat affected zone of 304 stainless steel during multipass welding

Xizhang Chen[1,2] · **Xing Chen**[2] · **Huili Xu**[2] · **Bruce Madigan**[3]

Received: 26 August 2014 / Accepted: 13 March 2015 / Published online: 16 April 2015

Abstract Grain growth in the weld heat-affected zone (HAZ) of multipass welds in 304 stainless steel was studied experimentally and theoretically. A finite element heat flow model was developed and calibrated using experimental temperature data collected during multipass gas tungsten arc welding. Output from the heat flow model was used to provide temperature data as an input to a Monte Carlo (MC) HAZ grain growth model and simulation adapted to multipass welds. The grain growth, grain size, and distribution in the HAZ predicted by the MC model were consistent with metallographic measurements of grains in the HAZ. Grains near the fusion boundary grew two to three times the size of grains in the unaffected base material. The MC model was then used to investigate the influence of initial base material temperature and interpass temperature on HAZ grain growth. As initial temperature increased, the width of the fusion zone in the first pass increased and the width of and grain size in the HAZ near the first pass increased. As interpass temperature increased, the width of the fusion zone and the width of and grain size in the HAZ increases after the first pass increased.

Keywords 304 Stainless steel · Multipass welding · HAZ · Grain growth · Monte Carlo · Preheat · Interpass

✉ Xizhang Chen
kernel.chen@gmail.com

[1] School of Mechanical and Electrical Engineering, Wenzhou University, Wenzhou 325035, China

[2] School of Material Science and Engineering, Jiangsu University, Zhenjiang 212013, China

[3] Montana Tech of The University of Montana, Butte, MT 59701, USA

1 Introduction

When joining thicker material sections using arc welding, weld joints are commonly filled with multiple small weld passes as opposed to a single large weld pass. Multipass welding reduces total weld heat input, and each subsequent pass can effectively heat-treat each previous pass. As a result, multipass welding affords control of weld fusion zone microstructure, grain size, residual stress, and therefore, final weld mechanical properties. However, the repetitive thermal cycling associated with multipass welding leads to grain growth in the always-solid weld heat-affected-zone (HAZ). Coarsened grains in HAZ potentially possess properties, such as strength, ductility, toughness, and corrosion resistance, which are dramatically different from grains in the fusion zone and base material. Therefore, it is important and of practical significance to predict the final grain size distribution in weld HAZ [1].

Computer simulation represents a highly efficient method to quantitatively assess HAZ grain growth. The Monte Carlo (MC) computational algorithm is a commonly used method to simulate the grain growth structure under isothermal conditions as in heat-treatment and under non-isothermal conditions as in welding [2–4]. Sista et al. [3] simulated the evolution of grain structure in the entire HAZ and demonstrated a linear relationship between grain size and welding heat input. Recently, Mohammad Amin et al. [4] used MC to simulate the effect of initial grain size on HAZ formation during laser surface melting. While various analytical and numerical models have been developed to study the effect of single-pass welding heat input on HAZ grain structure, few studies have addressed grain growth in multipass welding of austenitic stainless steels.

In this paper, experimental temperature measurements were obtained from thermocouples embedded in a plate subjected to multipass welding. These experimental temperatures were then used to calibrate an ANSYS heat flow model to produce a range of simulated multipass HAZ thermal cycles. The simulated thermal cycles were then used as a basis for a MC HAZ grain growth simulation. The experimental and simulated time-based temperature data were used to establish the relationship between real time, t, and the MC simulation time, t_{MCS}, using the experimental data based (EDB) model proposed by Gao et al. [5]. The MC simulation considered microstructure evolution and grain growth in HAZ during multipass welding, and the simulated results were compared with experimental results. Factors which might affect grain growth were studied in detail.

2 Experimental measurement and numerical simulation of the temperature fields in multipass welding

During actual welding, material temperature varies dramatically in time and space, and the material's thermophysical properties change with temperature. Additionally, the latent heat of fusion and heat from other phase transformations also change the distribution of the temperature field during welding. Therefore, the numerical simulation of the welding temperature field must encompass a highly nonlinear, transient heat conduction problem [6]. The simplifying assumptions made to create analytical models commonly used to calculate the welding temperature field produces results that are generally inconsistent with the actual welding conditions, so deviation between simulation results and actual measurements cannot be avoided, especially in the area near the weld pool. Deviation between the simulated and actual temperature fields is especially significant in multipass welding of thick plate. Therefore, the use of analytical models alone to produce thermal fields for subsequent simulations is impractical. However, the numerical finite element modeling (FEM) method can be used to capture material property changes with temperature, calculate transient heat flow conditions, and therefore yield simulated thermal fields that closely match those of actual multipass welding [7]. In this paper, the FEM analysis software ANSYS was utilized to develop a heat flow model for multipass welding of 304 stainless steel thick plate. The model in this investigation was calibrated with temperature data collected from experimental welds and then used to produce numerical representations, in time and space, of multipass weld thermal fields.

2.1 Experiment procedure

The material used in this experiment was 304 stainless steel plate with a chemical composition as shown in Table 1 and physical properties as shown in Table 2. It is a common stainless steel that widely used in the most of the industries due to the desirable properties [8].

Plate samples were 50 mm long and 40 mm wide with a thickness of 6 mm. The V-groove weld joint had a groove angle of 60° and a root opening of 2 mm, as shown in Fig. 1. The plates were manually welded using the gas tungsten arc welding (GTAW) process with argon shielding. Filler metal, machined into rod form directly from pieces of the base metal, was added to the joint. The joints were filled using a total of four weld passes sequenced as shown in the model geometry in Fig. 2. The initial preheat temperature was 20 °C and the interpass temperature was maintained at 200 °C. The nominal welding parameters are shown in Table 3 where I is the arc current; U is the arc voltage; speed is the welding travel speed, and η is the assumed arc heat transfer efficiency.

In order to calibrate and verify the numerical simulation results of the temperature field, the actual welding thermal cycles at different locations within the weld area were obtained using thermocouples recorded by a temperature recorder. As shown in Fig. 3, prior to welding, 2 mm diameter holes were drilled to a depth of 3 mm from the top plate surface at the locations indicated. Thermocouples were staked into the holes to measure temperature during welding.

After welding, the specimens were sectioned, mounted, and polished. Optical microcopy was used to photograph the HAZ at the midpoint along the weld length. Grain size measurements in the HAZ were conducted in the area corresponding to the MC simulation region.

2.2 Finite element method of the temperature field in multipass welding

2.2.1 Welding heat source model

The welding heat source model is an important part of the thermal numerical simulation for welding, and the selection of the heat source model not only affects the shape and size of the weld-pool in the simulation, but is also closely related to the accuracy of the welding temperature field simulation. Numerous researchers like M. A. Wahab [9], Andreas Iundback [10], and P. N. Sabapathy [11] have done a great deal of research on heat source modeling. Typically, a volumetric-type point heat source is used in multipass welding simulations. A more realistic surface heat source to simulate a welding arc is the double ellipsoidal heat source model proposed by Goldak [12]. The double ellipsoid heat source provides a wide variety of model parameters which can be tuned to control power density and distribution. By tuning the heat

Table 1 The chemical composition of 304 stainless steel (wt%)

C	S	P	Si	Mn	Cr	Ni	N
0.08	0.03	0.045	0.75	2	19	9	0.1

source parameters, it is possible to match the simulated weld pool size, shape, penetration, and heat flow to those measured experimentally. The double ellipsoidal heat source shown in Fig. 4 was employed in this simulation.

The double ellipsoid heat source model is composed of both front and rear semi-ellipsoids. The front ellipsoid heat source equation is described as:

$$q(x,y,z) = \frac{6\sqrt{3}f_1 Q}{abc_1\pi\sqrt{\pi}} \exp\left(-\frac{3x^2}{a^2} - \frac{3y^2}{b^2} - \frac{3z^2}{{c_1}^2}\right) \quad (1)$$

and the rear ellipsoid heat source equation is described as:

$$q(x,y,z) = \frac{6\sqrt{3}f_2 Q}{abc_2\pi\sqrt{\pi}} \exp\left(-\frac{3x^2}{a^2} - \frac{3y^2}{b^2} - \frac{3z^2}{{c_2}^2}\right) \quad (2)$$

The parameters a, b, c_1, and c_2 are geometric parameters of the double ellipsoid heat source model which express the shapes of the front and rear semi-ellipsoids. The parameters f_1, f_2 are coefficients expressing the power (heat input Q) distribution within the heat source where $f_1+f_2=2$ and generally $f_1=0.6$ and $f_2=1.4$.

The heat source dimensions and heat source parameters are usually determined by trial and error [13]. Initially, a set of values are selected based on the shape of the actual weld crater at the end of a weld pass. Those values are then used to run a simulation and produce a simulated thermal field. The simulated thermal field is then compared with the experimentally measured thermal field paying particular attention to the location and distribution of the weld fusion boundary. The heat source parameters are modified heuristically; the simulation is run again, and then the simulated thermal field is again compared with the experimental field. The heat source parameters are fixed when the simulated thermal field and location and distribution of the weld fusion boundary match those of the experimental welds. The heat source parameters used in this work are shown in Table 4.

Table 3 Welding parameters

Weld no.	I/A	U/V	Speed ($mm \cdot s^{-1}$)	η
1	75	11.0	0.6	0.7
2	85	12.5	0.5	0.7
3	75	11.2	0.55	0.7
4	75	11.2	0.55	0.7

2.2.2 Boundary conditions

During multipass welding and during the time between passes, thermal exchange occurs between the workpiece and its surroundings via conduction, convection, and radiation. Initial preheat and interpass temperatures have a significant influence on grain growth and therefore on mechanical properties of the weld. Control of preheat and interpass temperatures is an important part of a welding procedure specification. In this study, the influence of the different initial and interpass temperatures on the welding temperature field was considered within the simulation. The boundary conditions are as follows: the initial temperature T_a was set as 20, 100, and 300 °C and

Table 2 Physical properties of 304 stainless steels

Temperature, °C	Specific heat, $J \cdot kg^{-1} \cdot K^{-1}$	Heat conductivity coefficient, $W \cdot m^{-1} \cdot K^{-1}$	Density, $kg \cdot m^{-3}$
25	472	14.7	7,911
400	535	20.7	7,753
800	603	26.1	7,578
1,200	679	31.1	7,392
1,300	702	32.3	7,336
1,350	715	32.9	7,304
1,397	729	33.4	7,265
1,412	736	33.3	7,238
1,423	743	33.1	7,213
1,430	748	32.9	7,193
1,435	754	32.7	7,173
1,439	756	32.5	7,163
1,452	771	31.1	7,111
1,464	796	28.2	7,011
1,600	859	29.8	6,908

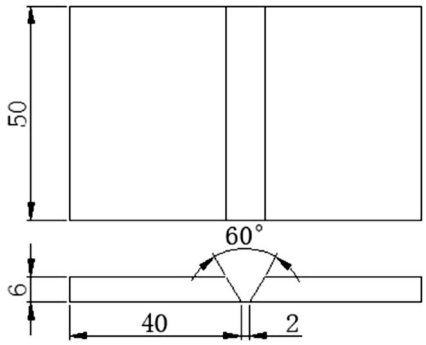

Fig. 1 Schematic diagram of weld joint configuration (dimensions in mm)

the interpass temperature was set at 100 °C, 200 °C, and 300 °C separately.

2.2.3 Simulation of multipass joint filling

In actual multipass welding of thick plates, the V groove joint is filled by adding molten filler metal to the weld pool pass after pass until the joint is full. The technique called element birth-death in the analyses is used to simulate the weld filler process with time [14]. In the simulation, all of the weld passes in the joint are first defined and made inactive. The first pass was then activated, and a solution was calculated. Then the next pass was activated, and all previous passes remained active, then a solution was calculated. The heat source was active only on the top-level pass each iteration. The process was repeated until all passes were activated and solved. Figure 5 shows the weld pass completion sequence used in the simulation.

2.3 Comparison of experimental and simulated welding thermal cycles

The heat flow model was developed, incorporating the material and heat source parameters, to produce simulated thermal fields that matched the experimentally measured thermal fields during multipass welding. Matching of the thermal fields was achieved through tuning the model parameters iteratively over many model runs until the simulated thermal fields were similar to the measured thermal fields over time and space. The simulated welding thermal cycles could then be obtained at various locations in the base plate relative to the weld fusion boundary. The thermal cycles were obtained from the model at the locations shown in Fig. 6, and the location coordinates are shown in Table 5.

As shown in Fig. 7, in general, the welding thermal cycles are characterized by a fast heating rate, high peak temperature, short residence time at high temperature, and a fast cooling rate. To provide a more detailed view of the simulated welding thermal cycle profiles for each weld pass at the prescribed joint locations, the horizontal ordinate (time) was divided into two parts for display. Figure 7a shows the simulated thermal cycle profiles from 0 s to 600 s, and Fig. 7b shows the thermal cycle profiles from 600 s to 1,200s. Each thermal profile contains four peaks, one for each weld pass as the heat source first approaches, and then moves past each joint location. For each weld pass, the temperature at each location starts at the preheat temperature, rises to a peak temperature, and decreases to the interpass temperature. At each location, peak temperature is a function of both distance from the location to the heat source during each weld pass, and the preheat and interpass temperatures.

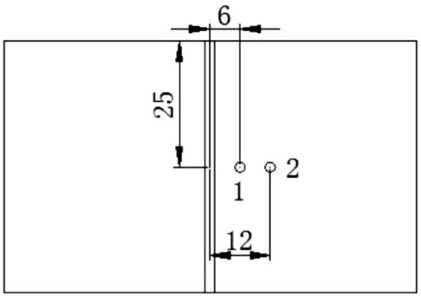

Fig. 3 Temperature measurement locations in the actual weld sample (dimensions in mm)

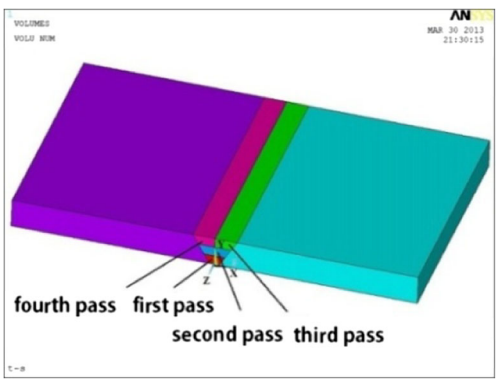

Fig. 2 Geometric weld model showing experimental and simulated weld pass sequence

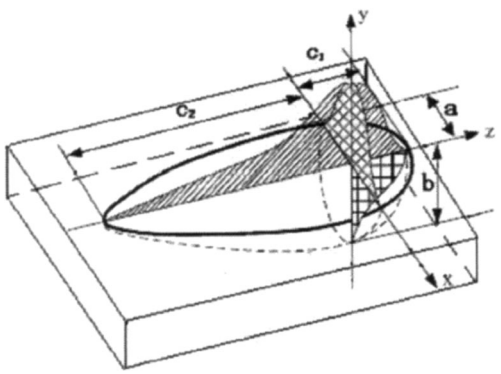

Fig. 4 Schematic diagram of double-ellipsoid heat source model

Table 4 The parameters of double ellipsoid heat source

Welding pass	a/mm	b/mm	c_1/mm	c_2/mm
1	4	2	3	8
2	5	2	3	8
3	3	3	3	8
4	3	3	3	8

Table 5 Coordinates of the model locations used to obtain simulated thermal cycles

Point no.	X (mm)	Y (mm)	Z (mm)
1	2.4	1	−25
2	3.5	3	−25
3	4.7	5	−25
4	7.0	5	−25

A comparison of the measured and simulated thermal cycles is shown in Fig. 8. In general, Fig. 8 shows good matching between the measured and simulated thermal cycles. There is some deviation between the measured and simulated results, especially in high-temperature regions. The reasons for the deviation can be explained as follows:

A. The sensitivity of the thermocouples decreases at higher temperature;
B. Modeling assumed the temperature field during welding was quasi-steady state; however, because the welded plates are relatively short in length, a quasi-steady condition was not fully realized;
C. The high temperature model parameters were obtained by linear interpolation and extrapolation and the actual material properties are non-linear by nature.

Nevertheless, the overall trend of the simulated thermal field is consistent with the measured thermal field which

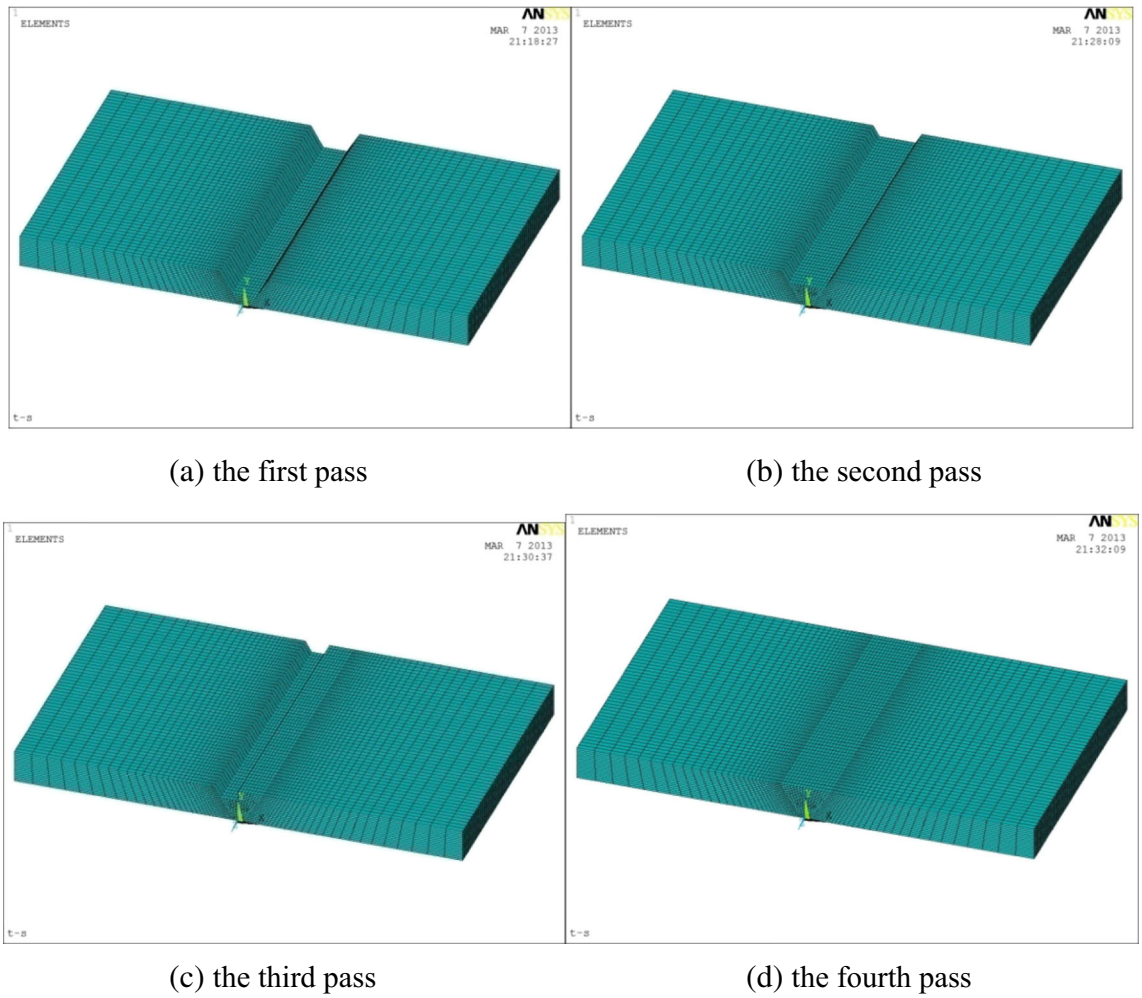

(a) the first pass (b) the second pass

(c) the third pass (d) the fourth pass

Fig. 5 The grain growth model weld pass activation sequence to fill the weld joint. **a** The first pass, **b** the second pass, **c** the third pass, and **d** the fourth pass

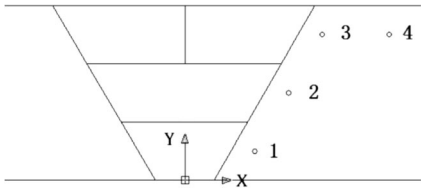

Fig. 6 Schematic diagram of model locations used to obtain simulated thermal cycles

shows that the numerical heat flow model is effective and can be used as the basis for numerical analysis of grain growth in HAZ.

3 MC simulation of grain growth in HAZ of multipass welding

Multipass welding can be considered as a cumulative process of multiple single-pass welds. Austenite stainless steel that do not undergo solid-state phase transformations, the accumulation of many single-pass welding thermal cycles, will inevitably cause grain coarsening in HAZ. 2D grain growth in the HAZ at the center of the weld length was simulated by the MC method. Multiple factors influencing grain growth were studied.

The development of a 2D MC model to simulate the grain growth involves incorporating many aspects of the physical problem including: the choice of the simulation region; simulation domain discretization; and the selection of initial and boundary conditions. The formulation and use of the MC technique to model grain growth in the HAZ of welds has been reported in various applications by other researchers [1, 3, 5, 15]. After a brief introduction to the MC grain growth methodology, the significant changes to adapt the existing body of work to multipass welding of 304 stainless steel are covered.

3.1 MC grain growth model

In this work, the microstructure near the weld fusion zone is simulated by creating a lattice structure in a 2D planar simulation region. The MC simulation region over which the lattice was mapped contains the weld pool, the HAZ, and the unaffected base plate as shown in Fig. 9. Assuming axial symmetry about the weld center line, only half of the weld area can be used as the computational domain. Furthermore, the simulation area is located mid-way along the length of the weld where the simulated temperature field is regarded as being quasi-steady state during welding, that is, the temperature field at the weld length center is not significantly influenced by the weld start and stop transient conditions.

Each point in the lattice is a called a site, S_i, and a total of N sites make up the lattice (site spacing on the order of 5 μm). The total number of sites is determined by the extent of the simulation region and the initial grain size, L_o, of the material under study. The lattice site density is set high enough such that multiple sites exist within each initial grain of the real material. Having multiple lattice sites within each grain allows for different regions within a single grain to experience

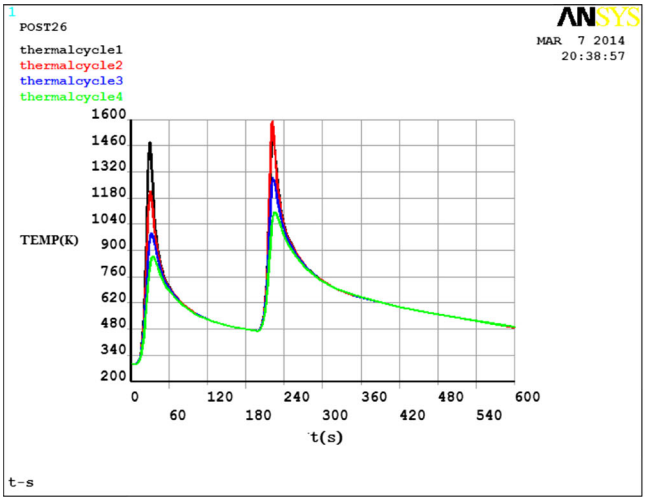

(a) The first half part of the thermal cycle curves (0-600s)

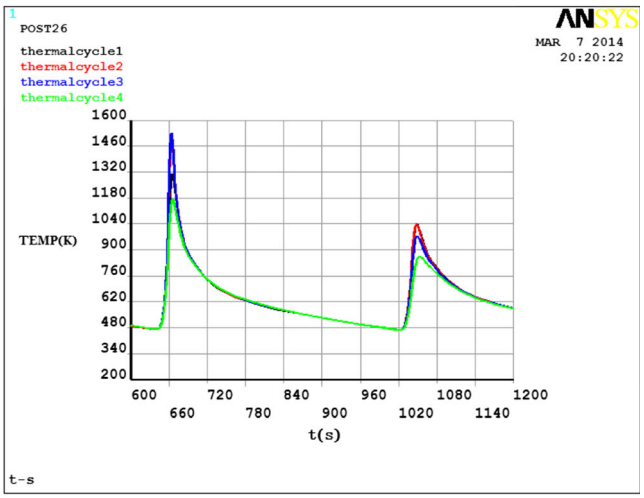

(b) The second half part of the thermal cycle curves (600-1200s)

Fig. 7 Welding thermal cycle for all 4 weld passes profiles from the heat flow simulation. **a** The first half part of the thermal cycle curves (0–600 s). **b** The second half part of the thermal cycle curves (600–1,200 s)

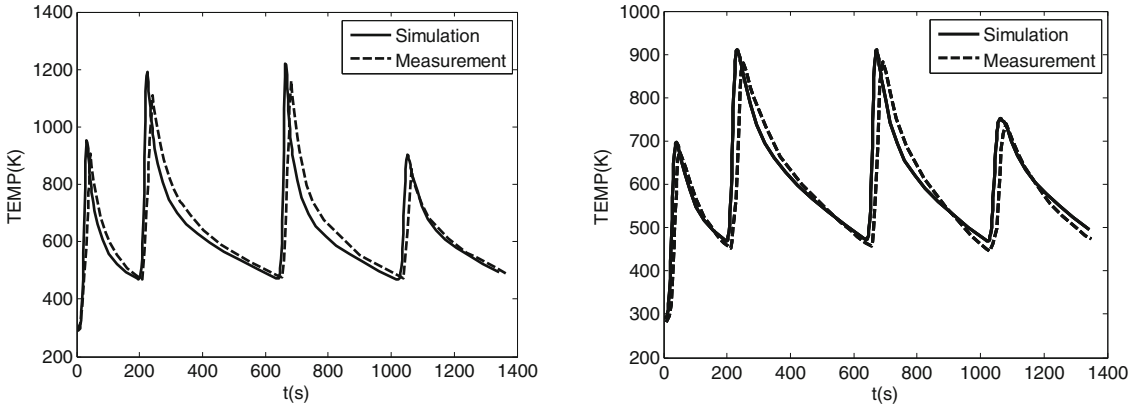

(a) Measured and simulated thermal cycles in Sample 1 (b) Measured and simulated thermal cycles in Sample 2

Fig. 8 Comparison of the measured and simulated thermal cycles. **a** Measured and simulated thermal cycles in sample 1. **b** Measured and simulated thermal cycles in Sample 2

different growth rates attributable to large thermal gradients that may exist across an individual grain. Each lattice site has eight nearest neighbors. Each site is also randomly assigned an orientation number. The orientation number has physical significance in that each grain in the material has a preferred growth direction relative to the thermal gradients caused by welding. In this work, each lattice site is initially assigned a random orientation number. The total possible solid-state orientation numbers range from 1 to X.X. The value of X.X. should not be too small; otherwise, the probability of the adjacent lattice for the same value will increase. Orientation number 0 is reserved for the liquid phase. Within the simulation area, a solid grain is a collection of neighboring lattice sites that share the same non-zero orientation number. Thus, grain boundaries exist at the interface between collections of sites with different orientation numbers. As in real materials, higher system energy is associated with grain boundaries compared with grain interiors.

Typically, the procedure for completing a time step in the MC method for grain growth consists of the following substeps [15]:

- Select a lattice site at random
- To this site, assign a randomly selected orientation number not equal to that presently assigned

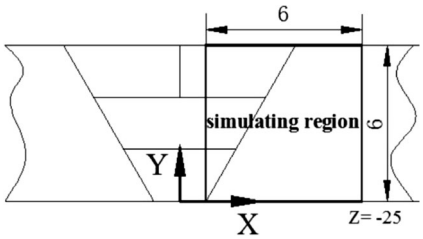

Fig. 9 MC Simulation region cross-section at the weld length center

- Calculate the net change in energy associated with grain boundary migration due to the site orientation number change
- Accept the attempted lattice reorientation if a reduction in overall system energy results; otherwise, reject the change and repeat the procedure at the next randomly selected lattice site.

The above procedure works on one lattice site at a time, which is unlike actual grain growth wherein changes occur at all sites simultaneously. In this work, the overall MC model is improved. First, a copy of the existing lattice is made. Orientation changes are made sequentially to the lattice copy. At each site in the lattice copy, if the orientation change reduces the system energy, the change at that site is stored in the copy, otherwise the change is rejected. After visiting all sites in the lattice copy, if the energy of the lattice copy is lower than that of the existing lattice, the lattice copy replaces the existing lattice and becomes the basis for the next gain growth iteration. If the energy of the lattice copy is greater than that of the existing lattice, the lattice copy is abandoned and the procedure begins again. The program flow chart of the simulation of the grain growth in HAZ is shown in Fig. 10.

3.2 The relation model between Monte Carlo simulation steps and the real time in HAZ

The simulation time, t_{MCS}, in MC model is not identical with real-time, t. Thus, a transformation relationship between the real time step t and MC time step, t_{MCS}, must be established to simulate the grain growth in the HAZ. MC time step, t_{MCS}, is expressed relative to t in terms of the simulated grain size with respect to the actual or real grain size. The relation between the

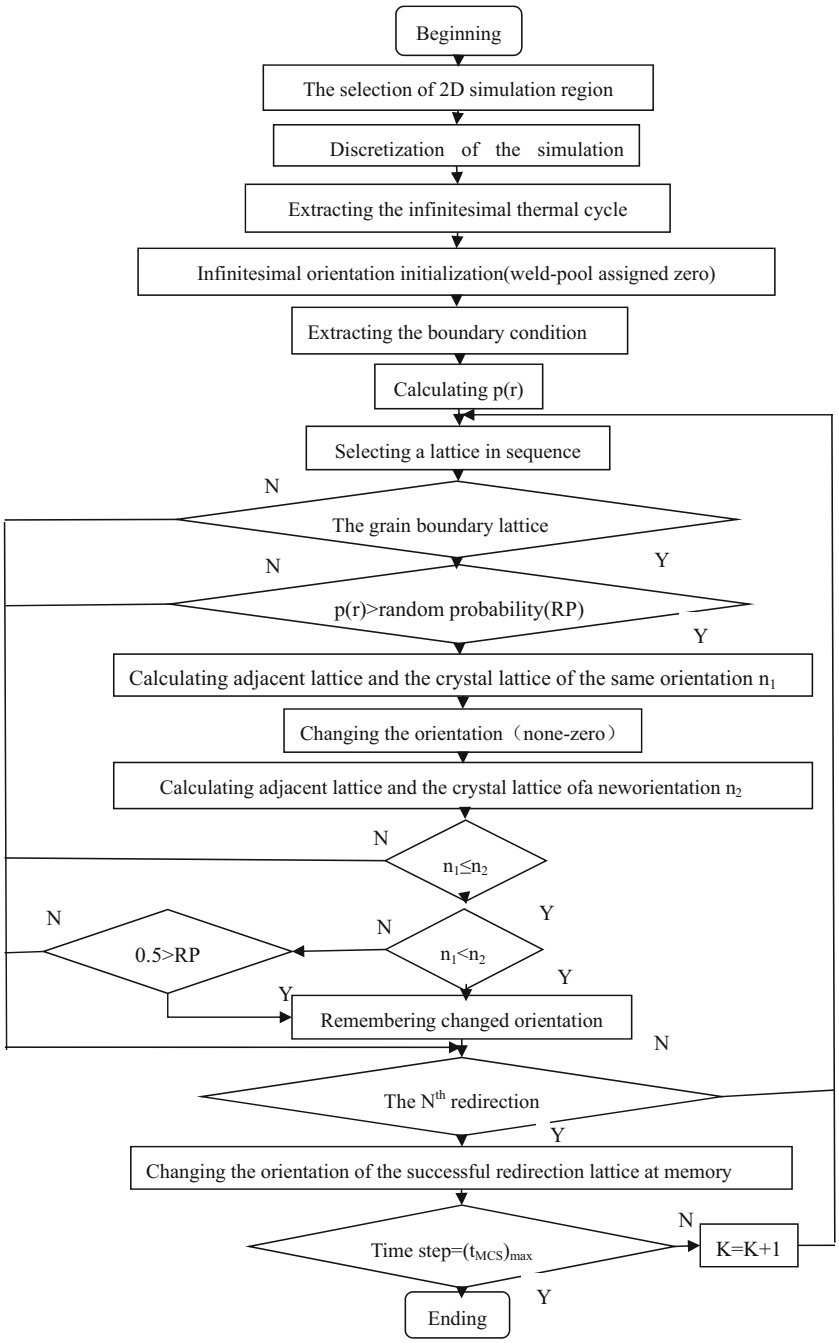

Fig. 10 Flow diagram of MC simulation of grain growth

Table 6 Parameters for HAZ grain growth simulation in 304 stainless steel in the EDB model

Physical	Symbol	Value
Grain growth index	n	0.25
Lattice site grid spacing (μm)	λ	5
Initial grain size (μm)	L_o	30
Model constant	K_1	7.7e5
Pre-exponential constant	K	1.2e14
Model constant	n_1	0.476
Universal gas constant (J/mol°K)	R	8.314
Grain growth activation energy (J/mol)	Q	2.1e5

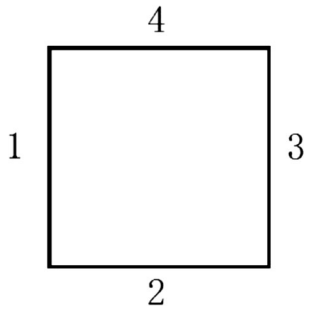

Fig. 11 The boundaries of simulation region. *1*: the left boundary is the fusion zone centerline; *2*: the lower boundary is the lower surface of the base plate; *3*: the right boundary is the unaffected base plate; and *4*: the upper boundary in the upper surface of the base plate

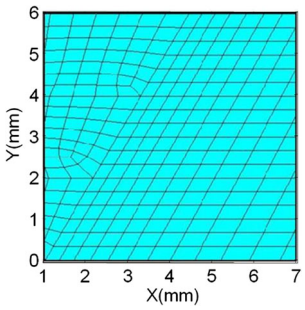

Fig. 12 Macroscopic ANSYS heat flow model temperature grid used to obtain temperature values for multipass weld thermal cycles imposed on the 6×6 mm grain growth simulation region

simulation time and real time is established via the EDB model in ref. [5]:

$$t_{\mathrm{MCS}} = \left\{ \frac{1}{K_1 \lambda} \left[K \sum_i \left[\exp\left(-\frac{Q}{RT_i} \right) \Delta t_i \right] + L_0^{\frac{1}{n}} \right]^n - \frac{1}{K_1} \right\}^{\frac{1}{n_1}} \quad (3)$$

where:

t_{MCS}	Monte Carlo time step
λ	lattice site grid spacing
K_1	a model constant
n_1	a model constant
n	grain growth exponent
K	pre-exponential constant
Q	grain growth activation energy
R	universal gas constant
Δt_{i}	small real-time interval
T_{i}	mean temperature in a small real-time interval Δ
L_0	the initial average grain size.

Numerical values for the parameters in the formula 8 were taken from ref. [16] and from measurements of the 304 stainless steel base plate used here, namely:

$$t_{\mathrm{MCS}} = \left\{ 0.26 \times \left[1.2 \times 10^{14} \sum \left[\exp\left(-\frac{2.526 \times 10^4}{T_i} \right) \Delta t_i \right] + 8.1 \times 10^5 \right]^{0.25} - 1.3 \right\}^{2.1} \quad (4)$$

Simulation model MC parameters used here are shown in Table 6.

3.3 Simulation region conditions

The HAZ grain growth simulation region contains boundaries at the weld centerline, the bottom of the base plate, the top of the plate, the unaffected base plate, and the fusion zone liquid–solid interface as shown in Fig. 11.

In areas of solid material where grain growth occurs, each lattice site is considered to have eight nearest-neighbor lattice sites. At the boundaries 1, 2, 3, and 4, the number of nearest-neighbor sites is less than 8. During the grain boundary energy calculations, fictitious lattice sites are introduced temporarily at the boundaries and assigned a lattice orientation number of zero [17]. Likewise, lattice sites that are above the melting temperature at the weld fusion zone boundary are assigned a lattice orientation number of zero. The zero orientation number means the energy change, before and after a reorientation attempt, associated with those lattice sites is 0.

3.4 Determination of temperature in the simulation region

The 6×6 mm cross-section at the grain growth simulation region was divided into a 1,200×1,200 square grid each with a lattice spacing of 5 μm. The temperature distribution in the simulation area is, relative to the grain growth, macroscopic in size, and can be modeled with a grid size (approximately 0.5 mm spacing) that is considerably coarser than the grid size of lattice sites. Figure 12 shows the temperature grid extracted

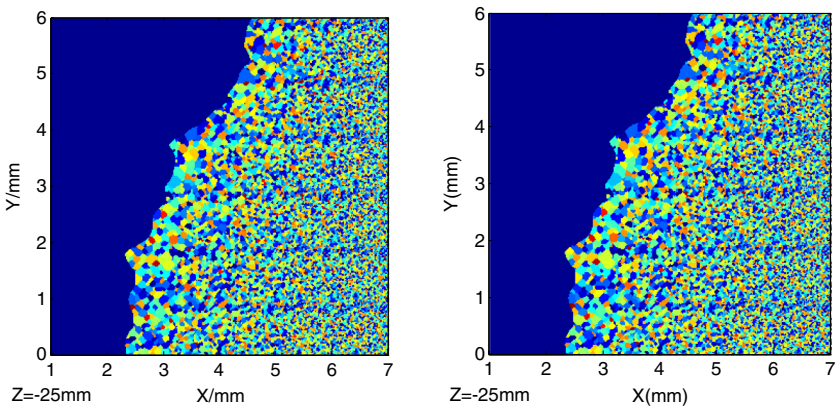

Fig. 13 Simulated grain size distribution in the HAZ after four weld passes (20 °C initial temperature and 200 °C interpass temperature and Table 3 welding parameters)

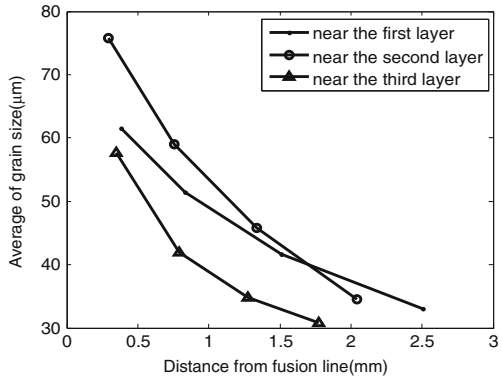

Fig. 14 Actual grain size distribution in the HAZ after 4 weld passes (20 °C initial temperature and 200 °C interpass temperature and Table 3 welding parameters)

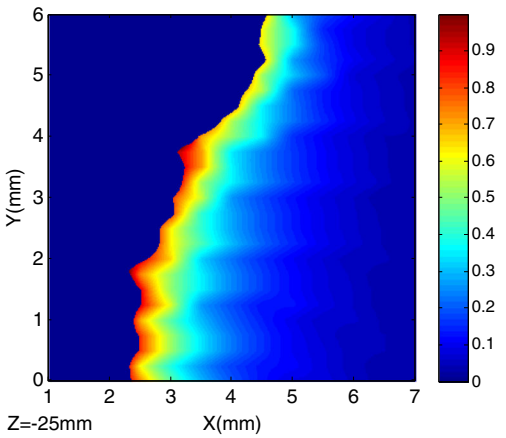

Fig. 16 The probability of model lattices sites experiencing larger values of t_{MCS}, and therefore greater grain growth decreases as distance away from the fusion boundary increases

from the heat flow model and imposed on the 6 mm×6 mm MC simulation region. The heat flow model allows the temperature to be known at each macro-level temperature grid node location as a function of time. To calculate temperatures on the much finer grain growth lattice grid (approximately 5 μm spacing), 3D temperature interpolation is used to obtain T_i at each MC model time step. While the interpolation calculation is expensive in terms of processing time, interpolation eliminates the need to store and recall huge amounts of temperature data from the heat flow model into the grain growth model.

4 Results and discussion

4.1 Simulation and experimental grain growth

The grain growth model was first executed with the same conditions used to produce the experimental weld, namely the welding parameters in Table 3, an initial preheat 20 °C and an interpass temperature of 200 °C. Grain sizes from the simulation are shown in Fig. 13 and from the actual weld specimen in Figs. 14 and 15.

As shown in Figs. 13, 14, and 15, grains in the near HAZ, close to the fusion zone, experience significant growth and achieve a large grain size, approximately two to three times the size of the grains in the unaffected base material. Grains in the far HAZ show less growth. Grain size decreases as distance from the fusion zone increases. Such behavior is consistent with grains nearer the fusion zone experiencing higher peak temperatures and longer high-temperature residence times compared with grains further from the fusion zone. The behavior is captured in the MC simulation through the probability of lattice sites nearer the fusion zone attaining a higher value of MC step time t_{MCS}. The higher the temperature and the longer time for grain growth at a site correspond to a higher value of t_{MCS} obtained from the equation in ref. [16]. Thus, lattice sites closer to the fusion boundary experience greater growth through a higher probability of attaining higher values of t_{MCS} as demonstrated in Fig. 16.

In addition, the grain growth situation within the HAZ of each weld pass zone is not the same. The width of the coarse-grained zone in the HAZ near the first weld pass is greater than that of the width near the second- and third-weld passes. The width of the HAZ and the degree of grain growth mainly depend on the peak temperature and the high-temperature

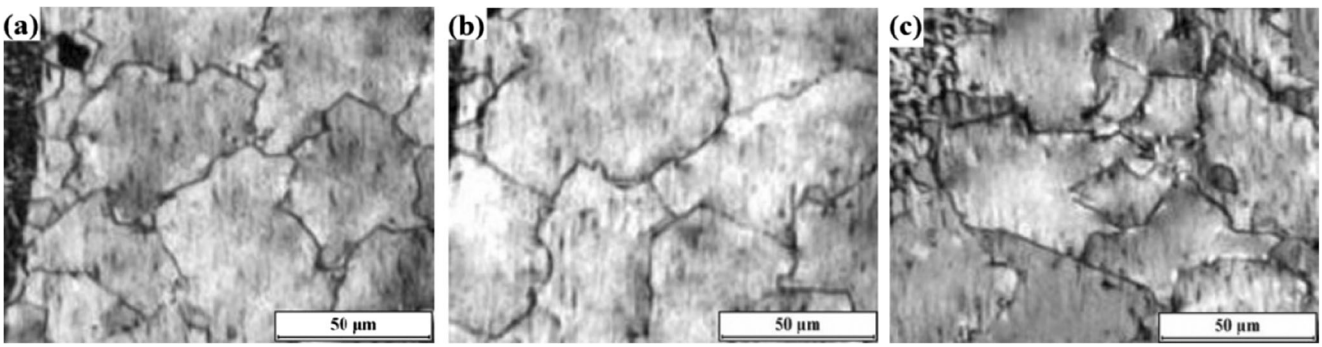

Fig. 15 Micrographs of HAZ grains in the HAZ at different weld passes: **a** first pass, **b** second pass, and **c** third pass (20 °C initial temperature and 200 °C interpass temperature and Table 3 welding parameters)

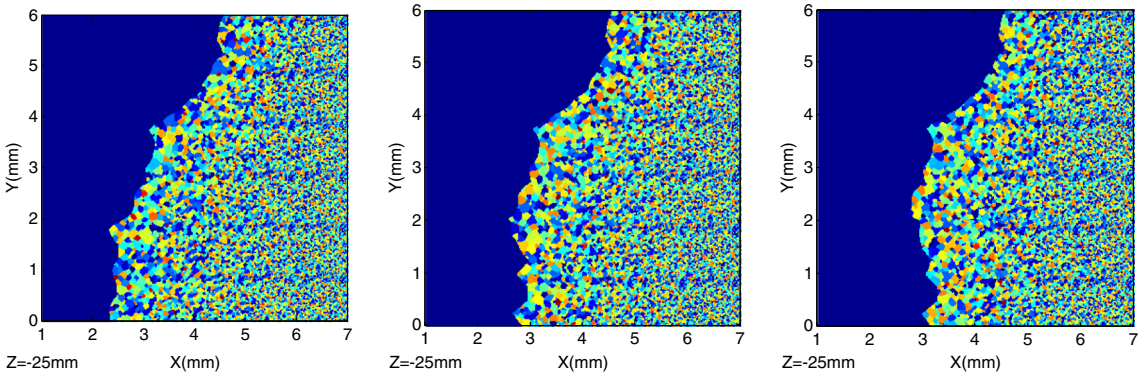

(a) 20°C initial temperature (b) 200°C initial temperature (c) 300°C initial temperature

Fig. 17 The simulated grain growth in HAZ under different initial pre-heat temperatures. **a** 20 °C initial temperature, **b** 200 °C initial temperature, and **c** 300 °C initial temperature

residence time afforded by the welding thermal cycle. Figures 7 and 8 show that HAZ near the first weld pass experiences a very high peak temperature during the first pass. During subsequent passes, the HAZ near the first pass experiences high peak temperatures, though not as high as that produced by the first pass. Thus the HAZ near the first pass has a higher probability of a large t_{MCS} due to the second, third and fourth passes. The situation is similar for the second pass. The HAZ of each pass is influenced by each subsequent pass. As shown in Figs. 13, 14, and 15, the grain size in HAZ near the second weld pass is larger than that of the other passes due to the slightly higher total heat input of the second pass (see Table 3).

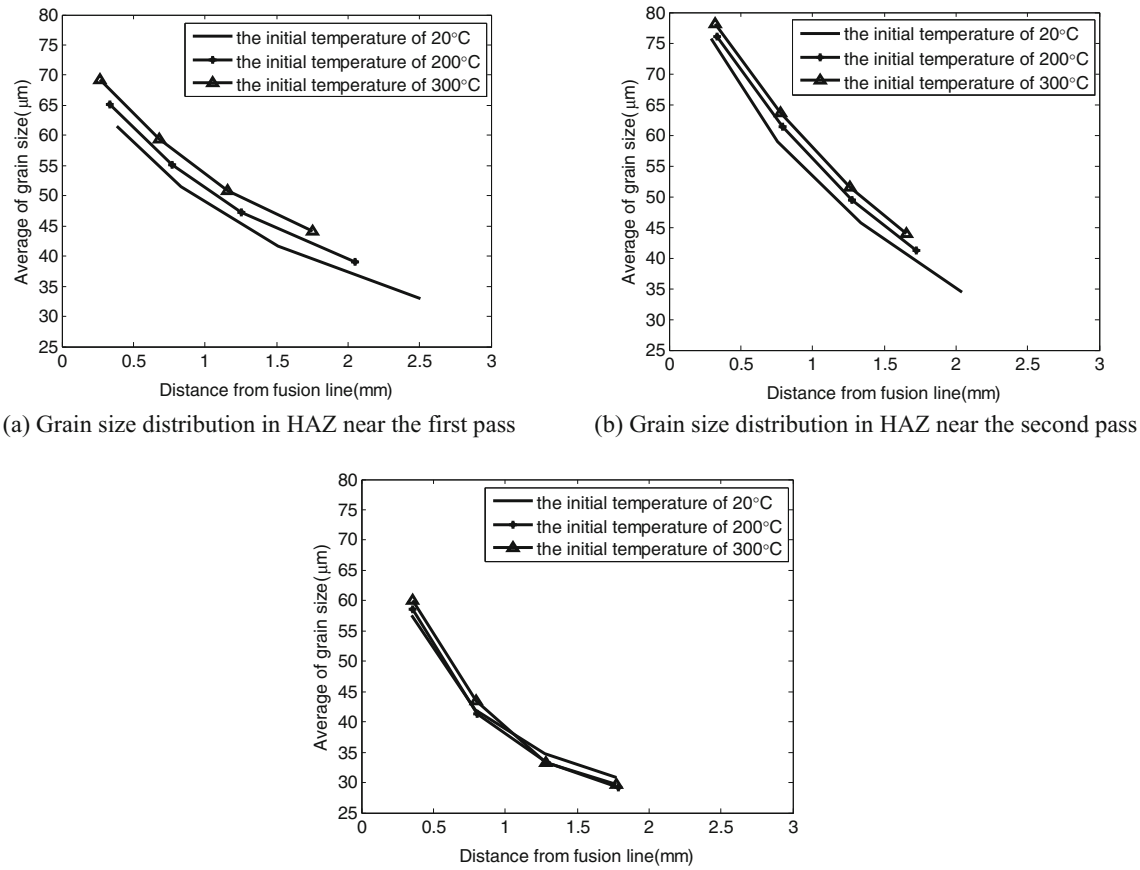

(a) Grain size distribution in HAZ near the first pass

(b) Grain size distribution in HAZ near the second pass

(c) Grain size distribution in HAZ near the third pass

Fig. 18 The grain size distribution in HAZ near weld passes under different initial preheat temperatures. **a** Grain size distribution in HAZ near the first pass. **b** Grain size distribution in HAZ near the second pass. **c** Grain size distribution in HAZ near the third pass

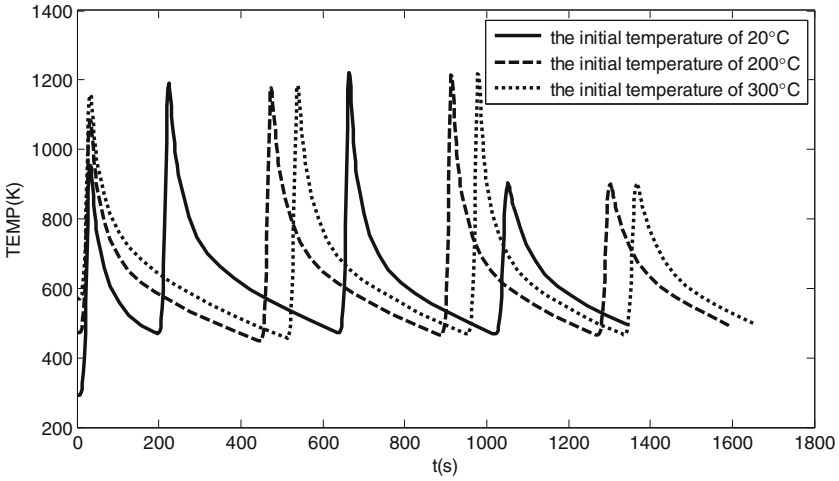

Fig. 19 The welding thermal cycle curves at simulation location 4 under different initial temperatures

The influence of the higher heat input for pass 2 can also be observed in the thermocouple and model temperature data. The consistent correlation between the experimental and simulated HAZ grain size and distribution indicates that the 2D MC model established here can be used to predict HAZ grain growth in multipass welding of 304 stainless steel.

4.2 The influence factors of the HAZ grain growth in multipass welding

Having established a consistent correlation between the experimental and simulated HAZ grain growth, the MC model was then exercised to study the influence of additional welding procedures parameters on HAZ grain growth without the need to make additional experimental welds. Such studies are useful not only to understand the influence of other factors but also to develop welding procedures to minimize grain growth in practical welding applications. The additional two factors affecting the grain growth in HAZ investigated here are initial preheat temperature and interpass temperature.

4.2.1 Influence of initial preheat temperature

In order to study the effect of the initial preheat temperature on the HAZ grain growth in multipass welding, the MC simulation model was executed with preheat temperatures of 20 °C, 200 °C, and 300 °C with the interpass temperature held at 200 °C. The results of the simulations are shown in Figs. 17 and 18.

Figure 17 shows that the fusion zone width of the first pass, with constant welding heat input, increases with preheat temperature. Furthermore, after the first pass, with constant interpass temperature, the fusion zone widths of the other passes do not change significantly with initial temperature. The effect of the initial temperature on the grain growth in HAZ near the first pass is obvious. The width of grain size within the first pass HAZ increases with the increasing of the preheat temperature. However, the width of grain size within the second- and third-pass HAZs does not change significantly. Numerical grain size data as a function of distance from the fusion boundary taken from the MC model and plotted in Fig. 18 demonstrate the same observations.

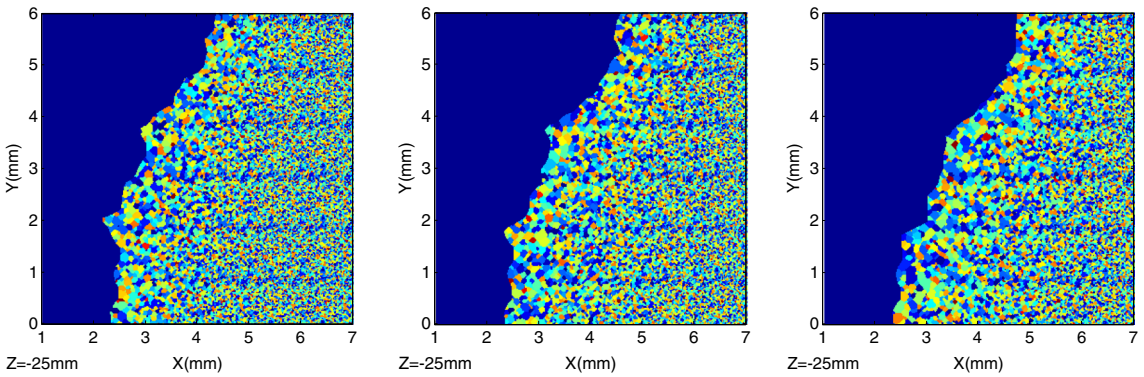

Fig. 20 The simulated grain growth in the HAZ under different interpass temperatures. **a** 100 °C interpass temperature, **b** 200 °C interpass temperature, **c** 300 °C interpass temperature

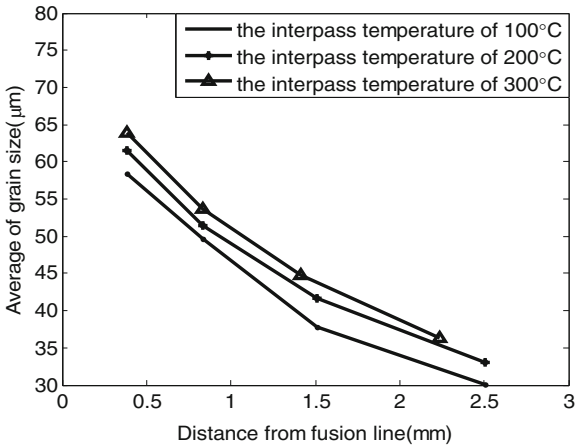

(a) Grain size distribution in HAZ near the first pass

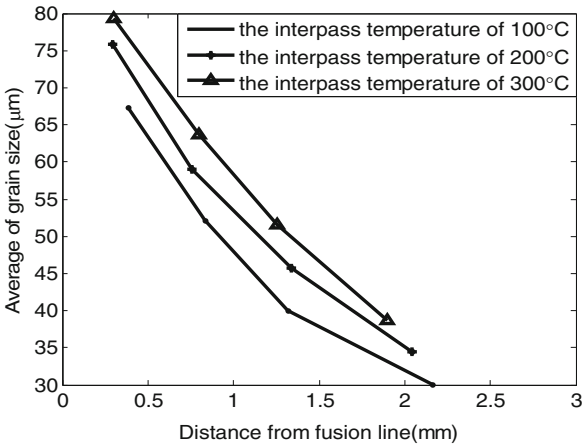

(b) Grain size distribution in HAZ near the second pass

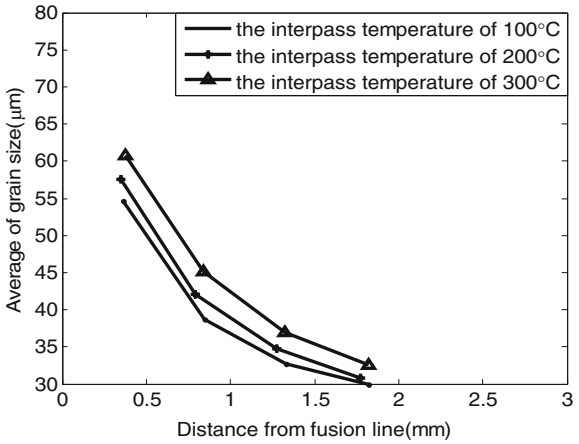

(c) Grain size distribution in HAZ near the third pass

Fig. 21 The grain size distribution in HAZ near weld passes under different interpass temperatures. **a** Grain size distribution in HAZ near the first pass, **b** grain size distribution in HAZ near the second pass

Figure 19 shows that the initial temperature influences only the welding thermal cycle of the first pass and not the thermal cycles of the subsequent passes because the interpass temperature was held constant. The higher initial preheat temperature

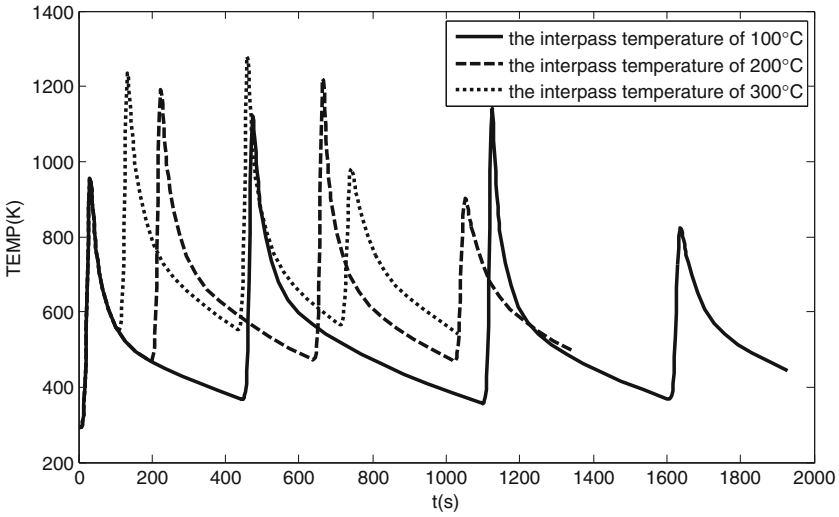

Fig. 22 The welding thermal cycle curves at simulation point 2 under different interpass temperatures

during the first weld pass leads to a higher peak temperature and longer residence time at high temperature, an increase in fusion zone width and a wider HAZ with larger grains compared with the subsequent passes.

4.2.2 Influence of interpass temperature

The interpass temperature for all passes beyond the first is equivalent to the preheat temperature for the first pass. In order to study the effect of interpass temperature on the HAZ grain growth in multipass welding, the MC simulation model was executed with interpass temperatures of 100, 200, and 300 °C and the initial preheat temperature held at 20 °C. The results of the simulations are shown in Figs. 20 and 21.

Figure 20 shows that the fusion zone width of the first pass is constant with constant welding heat input and constant preheat temperature, obvious because preheat temperature is only applicable after the first pass. Figure 20 also shows that the fusion zone width of the second and third passes increase with increasing interpass temperature. Furthermore, Fig. 20 shows the width of and grain size within the first-pass HAZ remain constant because the initial temperature is constant. However, the width of grain size within HAZs near the second and third passes increases with increasing interpass temperature. Numerical grain size data as a function of distance from the fusion boundary taken from the MC model and plotted in Fig. 21 demonstrate the same observations.

In order to analyze the influence of interpass temperature on the HAZ grain growth, simulation temperature data from location 2 ((3.5, 3, −25 mm) in Fig. 6 and Table 5) was extracted from the model and plotted in Fig. 22. It Figure 22 shows that, at location 2, the highest peak temperature in the HAZ occurs during the second pass for all interpass temperatures and the value of that peak temperature and the resident time at high-temperature increase with increasing preheat temperature. Also, the time between passes required for the workpiece to cool down to the interpass temperature decreases with increasing interpass temperature. The higher peak temperature and longer high-temperature residence time produced by higher interpass temperature lead to higher greater grain growth and larger fusion width in all weld passes beyond the first pass. Therefore, it is important to control the interpass temperature during multipass welding. Higher interpass temperature for all other welding parameters constant causes grain coarsening and increased fusion zone width and in general a reduction in most mechanical properties.

5 Conclusions

Grain growth in the HAZ of multipass welds in 304 stainless steel was studied experimentally and theoretically through numerical simulation. The following conclusions are drawn from this work:

1. A finite element heat flow model was developed and calibrated using the experimental temperature data collected during multipass GTAW. Output from the heat flow model provided a convenient and rich temperature data set accurately reflecting the repetitive thermal history experienced by the grains in the HAZ
2. A MC model and simulation was developed and adapted to study grain growth in multipass welds using temperature data from the heat flow model. The grain growth and grain size and distribution in the HAZ predicted by the MC model were consistent with metallographic measurements of grains in the HAZ. Grains near the fusion boundary grew two to three times the size of grains in the unaffected base material.
3. The MC model was used to investigate the influence of a range of base material initial temperatures. As initial preheat temperature increased, the width of the fusion zone in the first pass increased and the width of and grain size within the HAZ near the first pass increased.
4. The MC model was used to investigate the influence of a range of base material interpass temperatures. As interpass temperature increased, the width of the fusion zone and the width of and grain size within the HAZ increased in passes after the first pass.
5. The approach taken to create the MC grain growth model here is extendable to other joint designs and alloy systems and may be useful for exploring the influence of a large range of common welding parameters without the need for extensive experimental investment.

References

1. Zhang SX, Liu XT, Wen JQ (2003) Monte Carlo computer simulation method of the microstructure evolution in HAZ. Electr Weld Mach 33(4):1–4
2. Anderson MP, Grest GS, Srolovitz DJ (1989) Computer-simulation of normal grain-growth in 3 dimensions. Philos Mag B Phys Condens Matter Stat Mech Electron Opt Magn Prop 59(3):293–329
3. Sista S, Yang Z, DebRoy T (2000) Three-dimensional Monte Carlo simulation of grain growth in the heat-affected zone of 2.25Cr-1Mo steel weld. Metall Mater Trans B 31B:529–536
4. Jabbareh MA, Assadi H (2013) Modeling of grain structure and heat-affected zone in laser surface melting process. Metall Mater Trans B Process Metall Mater Process Sci 44(4):1041–1048
5. Gao J, Thompson RG (1996) Real time-temperature models for Monte Carlo simulations of normal grain growth. Acta Mater 44(11):4565–4570
6. Wang JH (2003) Welding numerical simulation technology and its applications. Shanghai Jiao Tong University Press, Shanghai
7. Yang KC, Li CF, Wang YQ, Hu ZQ, Yang Y, Chen QY (2012) Application of ANSYS finite element simulation in welding temperature field analysis. Foundry Technol 33(6):718–720
8. Aval HJ, Farzadi A, Serajzadeh S, Kokabi AH (2009) Theoretical and experimental study of microstructures and weld pool geometry during GTAW of 304 stainless steel. Int J Adv Manuf Technol 42: 1043–1051

9. Wahab MA, Painter MJ, Davies MH (1998) The prediction of the temperature distribution and weld pool geometry in the gas metal arc welding process. J Mater Process Technol 77(1):233–239
10. Iundback A (2000) Modeling of weld path for use in simulations. LULEALUNBERSIT-Y OF TECHNOLOGY
11. Sabapathy PN, Wahab MA, Painter MJ (2000) The prediction of burn-through during in-service welding of gas pipelines. Int J Press Vessel Pip 77(11):669–677
12. Goldak J, Chakravarti A, Bibby M (1985) IIW Doc. No. 212-603-85
13. Varghese VMJ, Suresh MR, Suresh MR (2013) Recent developments in modeling of heat transfer during TIG welding—a review. Int J Adv Manuf Technol 64:749–754
14. Chen BQ, Hashemzadeh M, Soares CG (2014) Numerical and experimental studies on temperature and distortion patterns in butt-welded plates. Int J Adv Manuf Technol 72:1121–1131
15. Shen MD (2005) Monte Carlo simulation of grain growth in HAZ of X70 pipeline steel. Huazhong University of Science and Technology, China
16. Jamshidi AH, Serajzadeh S, Kokabi AH (2009) Prediction of grain growth behavior in HAZ during gas tungsten arc welding of 304 stainless steel. J Mater Eng Perform 18(9):1193–1200
17. Xiao J (2006) 3D simulation of grain growth in welding heat affected zone by Monte Carlo technique. Harbin Institute of Technology, China